FULL PAPER

Porous Nanofilm Biomaterials Via Templated Layer-by-Layer Assembly

Connie Wu, Seyma Aslan, Adeline Gand, Joseph S. Wolenski, Emmanuel Pauthe, and Paul R. Van Tassel**

Hydrogel-like biomaterials are often too soft to support robust cell adhesion, yet methods to increase mechanical rigidity (e.g., covalent cross-linking the gel matrix) can compromise bioactivity by suppressing the accessibility or activity of embedded biomolecules. Nanoparticle templating is reported here as a strategy toward porous, layer-by-layer assembled, thin polyelectrolyte films of sufficient mechanical rigidity to promote strong initial cell adhesion, and that are capable of high bioactive species loading. Latex nanoparticles are incorporated during layer-by-layer assembly, and following 1-ethyl-3-[3-dimethylaminopropyl]carbodiimide/*N*-hydroxysulfosuccinimide (EDC-NHS) cross-linking of the polyelectrolyte film, are removed via exposure to tetrahydrofuran (THF). THF exposure results in only a partial reduction in film thickness (as observed by ellipsometry), suggesting the presence of internal pore space. The attachment, spreading, and metabolic activity of pre-osteoblastic MC3T3-E1 cells cultured on templated, cross-linked films are statistically similar to those on non-templated films, and much greater than those on non-cross-linked films. Laser scanning confocal microscopy and quartz crystal microgravimetry indicate a high capacity for bioactive species loading (ca. 10% of film mass) in nanoparticle templated films. Porous nanofilm biomaterials, formed via layer-by-layer assembly with nanoparticle templating, promote robust cell adhesion and exhibit high bioactive species loading, and thus appear to be excellent candidates for cell-contacting applications.

1. Introduction

Nanoscale films formed via the layer-by-layer (LbL) assembly of oppositely charged macromolecular species[1] are finding widespread application in energy, sensing, and biomedicine.[2,3] LbL films are particularly attractive for applications involving contact with living cells or tissues– e.g., cell culture, tissue engineering, biomedical implants– since film chemical, mechanical, and biological properties may be tailored to promote a desired cellular response.[4–7] Initial cell adhesion generally increases with film rigidity, a material property enhanced through ionic or covalent cross-links.[8–23] Cell behavior may be further influenced through embedded biomolecules (e.g., growth factors, genetic material),[15,24–36] but chemical cross-linking, while tending to promote cell or tissue integration, may act to suppress film bioactivity by diminishing intrafilm biomolecular mobility[9,24,26] and/or cell-induced film degradation (hence limiting bioactive agent exposure to contacting cells),[9,37,38] or by chemically altering the film-embedded species.[15] A key challenge in nanofilm (and other hydrogel-like) biomaterial systems is to simultaneously achieve i) sufficient mechanical rigidity so as to promote strong initial cell adhesion and ii) a significant loading capacity for accessible, functionally active biomolecules.

We present here a nanoparticle templating strategy aimed at decoupling film rigidity from bioactivity. The idea is to embed nanoparticle templates within a LbL film, chemically cross-link the film to increase its rigidity, remove the template species through dissolution, and then load the resulting pore space with bioactive species. The goal is to produce films of sufficient mechanical rigidity to promote a robust initial cell response, while maintaining a high loading of functional and accessible bioactive species. Templating in the context of LbL assembly typically involves film formation around a core particle, which upon dissolution leaves a dense, spherical polyelectrolyte shell surrounding an empty space;[39–41] the idea to template the interior of the film itself with sacrificial species originates with the work of Caruso, et al.[42,43] Our strategy builds upon this latter approach, with a goal of films that are simultaneously

C. Wu, Dr. S. Aslan, Prof. E. Pauthe, Prof. P. R. Van Tassel
Department of Chemical and Environmental Engineering
Yale University
New Haven, CT 06520-8286, USA
E-mail: emmanuel.pauthe@u-cergy.fr; paul.vantassel@yale.edu
A. Gand, E. Pauthe,
Equipe de Recherche sur les Relations Matrice Extracellulaire Cellules
Institut des Matériaux
Université de Cergy-Pontoise
Cergy-Pontoise Cedex 95302 France
Dr. J. S. Wolenski
Department of Molecular, Cellular, and Developmental Biology
Yale University
New Haven, CT 06520-8103, USA

DOI: 10.1002/adfm.201201042

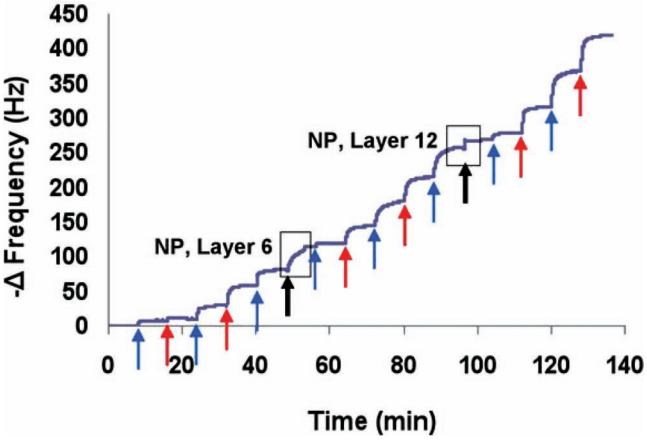

Figure 1. Quartz crystal microgravimetry with dissipation (QCMD) sensogram demonstrating layer-by-layer assembly of poly(L-lysine) (PLL) with poly(L-glutamic acid) (PGA) and carboxy functionalized latex nanoparticles (NP) (NP concentration 0.1 g/L). Blue, red, and black arrows indicate exposure to PLL, PGA, and NP, respectively. Frequency change indicates addition of mass to the film.

mechanically rigid and bioactive, and hence ideal for a range of biomaterial applications. In this article, we introduce nanoparticle templated LbL films exhibiting cell contacting properties comparable to their non-templated counterparts, and offering high loading capacity for biomolecular species.

2. Results

Homopolymers composed of charged amino acids represent a promising platform toward biocompatible, biodegradable nanofilm biomaterials, with abundant functional groups for chemical modification (such as cross-linking). In **Figure 1**, we show a quartz crystal microgravimetry with dissipation (QCMD) sensogram demonstrating the LbL assembly of (cationic) poly(L-lysine) (PLL) and (anionic) poly(L-glutamic acid) (PGA). At the sixth and the twelfth layers, PGA is replaced by a 0.1 g/L solution of carboxy functionalized latex nanoparticles (NP) of diameter 28 ± 4 nm. The sensogram demonstrates successful LbL assembly, and shows significant NP adsorption at the sixth layer, and modest NP adsorption at the twelfth layer. Employing a Voigt model of a viscoelastic polymer-NP film (see Experimental Section), we find NP loadings of 0.76 and 0.16 μg/cm^2 (or 630 and 130 NP/μm^2) in the 6th and 12th layers, respectively. Film assembly at a higher NP concentration (1 g/L) results in a much higher NP loading: 5.5 and 1.1 μg/cm^2 (or 4600 and 890 NP/μm^2), respectively, in the 6th and 12th layers. The equivalent 2-D fractional areas covered may be calculated as $\theta = 3\Gamma/2\rho d$, where Γ is the NP adsorbed mass per area, ρ is the NP density, and d is NP diameter. At NP concentration 0.1 g/L, θ = 0.39 and 0.08, in the 6th and 12th layers, respectively. These values, being smaller than the 2D closed packing limit, suggest the possibility of vertical NP confinement. At NP concentration 1 g/L, θ = 2.8 and 0.56, in the 6th and 12th layers, respectively. The former value clearly indicates the NP to distribute vertically to a significant extent throughout the film.

Table 1. Ellipsometry measurements of mean thicknesses of [(PLL-PGA)$_2$-PLL-NP]$_2$-(PLL-PGA)$_2$ films, with (XL) and without (Native) an EDC-NHS cross-linking treatment, and with and without a THF NP dissolution step, for various bulk NP concentrations.

	Native/no THF	Native/THF	XL/no THF	XL/THF
0 g/L NP	160 ± 20 nm	180 ± 20 nm	200 ± 20 nm	190 ± 20 nm
0.01 g/L NP	200 ± 20 nm	170 ± 20 nm	200 ± 20 nm	180 ± 20 nm
0.1 g/L NP	200 ± 20 nm	170 ± 20 nm	280 ± 20 nm	230 ± 20 nm
1 g/L NP	370 ± 20 nm	190 ± 20 nm	510 ± 20 nm	420 ± 20 nm

Following LbL assembly, a film is subjected to i) 1-ethyl-3-[3-dimethylaminopropyl]carbodiimide/*N*-hydroxysulfosuccinimide (EDC-NHS) chemical cross-linking agents and then ii) tetrahydrofuran (THF) to dissolve the embedded NP. EDC-NHS applied to PLL-PGA films has been shown previously to yield amide cross-links between amine groups on PLL and carboxyl groups on PGA, as observed by Fourier transform infrared spectroscopy in attenuated total reflection mode.[11,23] In **Table 1**, we show film thickness values measured via ellipsometry, as a function of NP concentration, with and without chemical cross-linking and THF exposure. The thickness of native films (i.e., without cross-linking) increases with NP concentration, but subsequent exposure to THF essentially suppresses this effect, suggesting removal of the NP and collapse of the film. Cross-linking enhances film thickness, and the NP concentration dependence remains. Exposure of a cross-linked film to THF also results in a thickness decrease, but in this case the final thickness exhibits a clear NP concentration dependence, suggesting only a partial collapse in the film, and hence the presence of open pore space following template removal. NP volume fraction, $\phi = \Gamma/\rho\, t_F$, may be calculated from the QCMD measured NP adsorbed mass (Γ) and the ellipsometry measured film thickness (t_F). We find NP volume fraction, a measure of porosity prior to NP dissolution, to be 3.1% and 12% for NP concentrations 0.1 and 1 g/L, respectively (for cross-linked films).

In **Figure 2**, we show atomic force microscopy images and cross-sectional profiles of a cross-linked film without NP, a native film with NP, and a cross-linked film with NP subsequently exposed to THF (i.e., a templated film). The cross-linked film without NP exhibits domains of approximate lateral diameter 20–50 nm and height 10–20 nm, and a root mean square roughness of 7 nm. The native film (not shown) displays similar topography, and an essentially equal roughness (8 nm). The native film with NP exhibits somewhat larger domains: 50–200 nm lateral diameter and 15–25 nm height. No direct evidence of the 28 nm diameter NP is observed, although some of the smaller domains could be individual NP, of larger apparent size owing to a tip broadening effect. The roughness of the NP film, 13 nm, is greater than those of the native or cross-linked films without NP. The relatively small increase in film roughness and domain size brought about by the presence of the NP suggests the absence of large scale NP aggregation within the film. Interestingly, the cross-linked film with NP and exposure to THF appears to have somewhat smaller domain sizes than the native film with NP, and has roughness (10 nm) intermediate between those of films with and without NP, suggesting NP removal to

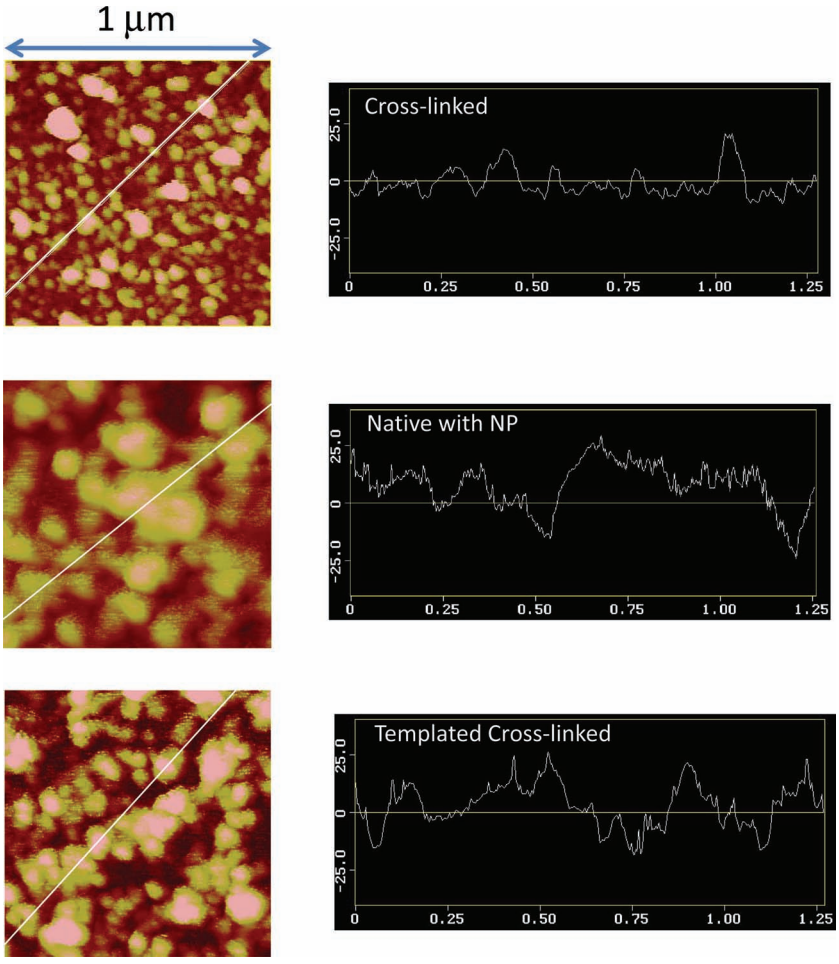

Figure 2. Left: Atomic force microscopy images of $(PLL\text{-}PGA)_{14}$ plus EDC/NHS chemical cross-linking (cross-linked), $[(PLL\text{-}PGA)_5\text{-}PLL\text{-}NP]_2\text{-}(PLL\text{-}PGA)_2$ (native with NP), and $[(PLL\text{-}PGA)_5\text{-}PLL\text{-}NP]_2\text{-}(PLL\text{-}PGA)_2$ plus EDC/NHS chemical cross-linking plus THF (templated cross-linked) films. Right: Cross sectional height profiles through the white line in the AFM images (vertical axis in nm, horizontal axis in μm). Films formed at NP concentration 1 g/L.

result in a modest film smoothing effect. It is important to note that all these films are quite smooth, with roughness values always less than 5% of film thickness (Table 1). For comparison, the underlying glass substrate exhibits a root mean square roughness of 10 nm.

Chemical cross-linking of LbL films generally improves the initial cellular response.[8–23] To test whether the templated films of this study exhibit such an improvement, we measure the attachment, spreading, and metabolic activity of pre-osteoblastic MC3T3-E1 cells on a native film without NP (negative control 1), a native film with NP (negative control 2), a cross-linked film without NP (positive control), and a cross-linked film with NP subsequently exposed to THF (i.e., a templated film). MC3T3-E1 is a well-established cell line known to be exhibit substrate rigidity-dependent adhesion, and to respond to various bioactive agents.[44,45] In addition, it represents a highly relevant progenitor cell system for bone tissue engineering–one of the envisioned applications of porous nanofilm biomaterials.[46] In **Figure 3**, we show the number of attached cells, following 3 h exposure time, to be similar on templated versus non-templated cross-linked substrates, and in both cases to be significantly higher than on films without cross-linking. Similar results are found in terms of degree of cell spreading following 24 h exposure: cells on both templated and non-templated cross-linked films exhibit a projected area nearly four times larger than do cells on native films (**Figure 4**). Optical microscopy images (Figure 4) show cells on a templated, cross-linked film to exhibit better organized actin cytoskeletons, and larger stress fibrils, compared to cells on a native film. Cellular metabolic activity may be measured via an alamar blue assay of mitochondrial activity. In **Figure 5**, we show the mitochondrial activity of cells on chemically cross-linked, templated films to be comparable to that on chemically cross-linked films without templates, and to be significantly greater than that on native films. Interestingly, the presence of NP in native films also leads to a significant increase in mitochondrial activity, although not to the level of the cross-linked films. NP additives have been shown to increase LbL film rigidity,[47] and are shown here (Figure 2) to increase LbL film roughness. Since both substrate rigidity and roughness have previously been correlated with increased mitochondrial activity,[48,49] we conclude one of these two effects to cause the increase observed here. In all, these cell results suggest templated, cross-linked films to promote cell adhesion and viability at a level similar to that of non-templated, cross-linked films, and at a level significantly higher than that of native films.

To investigate biomolecular loading within the templated pore space, we employ laser scanning confocal microscopy on films containing fluorescently labeled polymer, and subsequently exposed to a fluorescently labeled model biomolecular species, bovine serum albumin. In **Figure 6**, we show (cross-sectional) laser scanning confocal microscopy images of a $[(PLL\text{-}PGA)_5\text{-}PLL\text{-}NP]_4\text{-}(PLL\text{-}PGA)_2$ film, following EDC-NHS cross-linking, with the PLL in the penultimate layer containing a AF-488 (green) fluorescent label. Note that the film considered here contains more layers than those described above. The additional layers are needed to optically resolve the presence of bioactive species within the film. As noted previously, a certain fraction of labeled polymer diffuses freely within the film in the vertical direction;[50] hence, the entire film appears green. From these images, we observe film thickness to be about 8 μm.

Without the THF dissolution step (left of Figure 6), exposure to AF-568 (red) labeled albumin results in the film appearing green and the solution above the film appearing red, with no evidence of albumin penetration. Rinsing acts to remove most, but not all, of the red color, suggesting some albumin to remain adsorbed to the film surface. With the THF

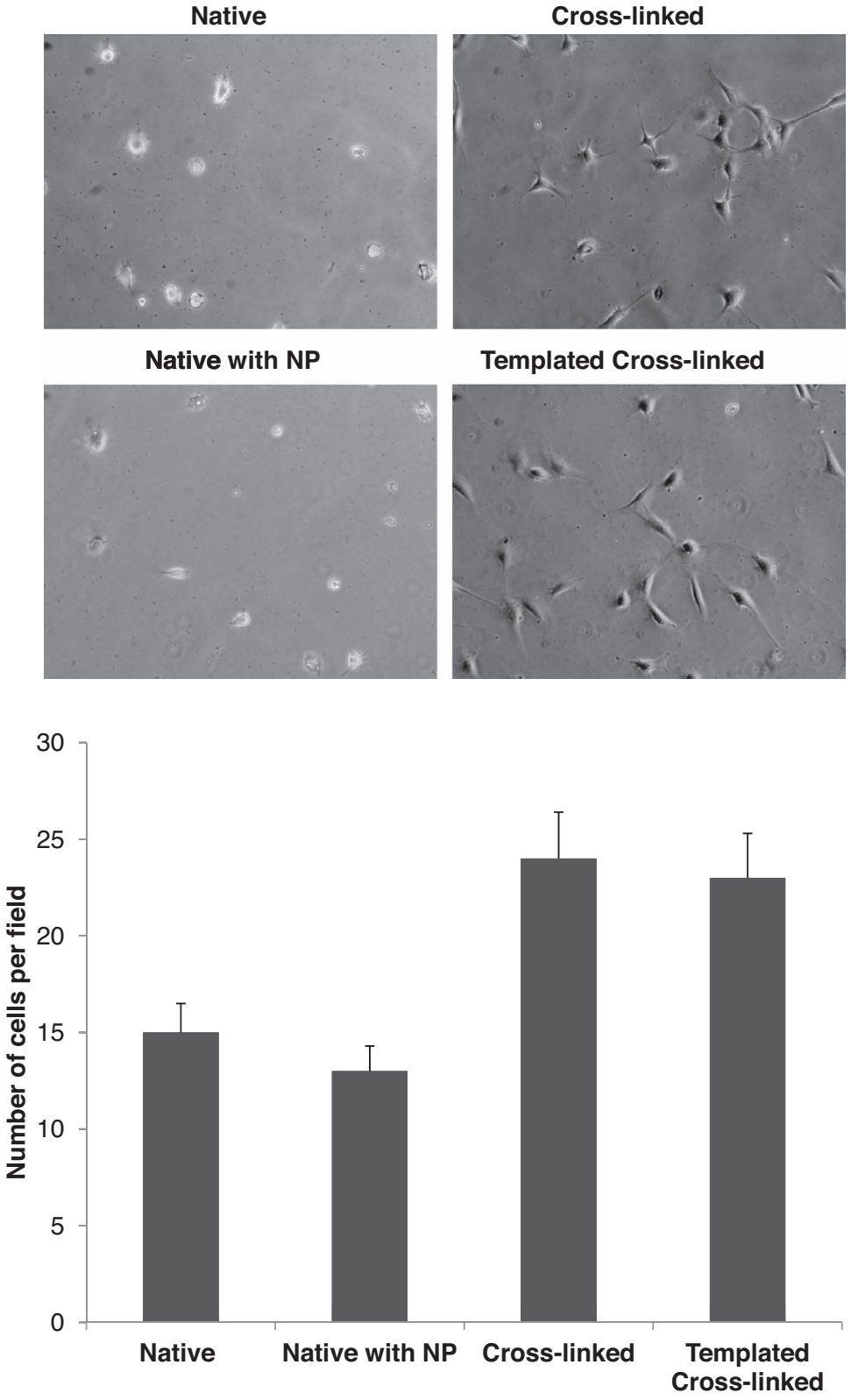

Figure 3. Optical microscopy images of MC3T3-E1 preosteoblast cells following 3 h culture on $(PLL\text{-}PGA)_{14}$ (native), $[(PLL\text{-}PGA)_5\text{-}PLL\text{-}NP]_2\text{-}(PLL\text{-}PGA)_2$ (native with NP), $(PLL\text{-}PGA)_{14}$ plus EDC/NHS (cross-linked) and $[(PLL\text{-}PGA)_5\text{-}PLL\text{-}NP]_2\text{-}(PLL\text{-}PGA)_2$ plus EDC/NHS plus THF (templated cross-linked) films. Films formed at NP concentration 0.1 g/L.

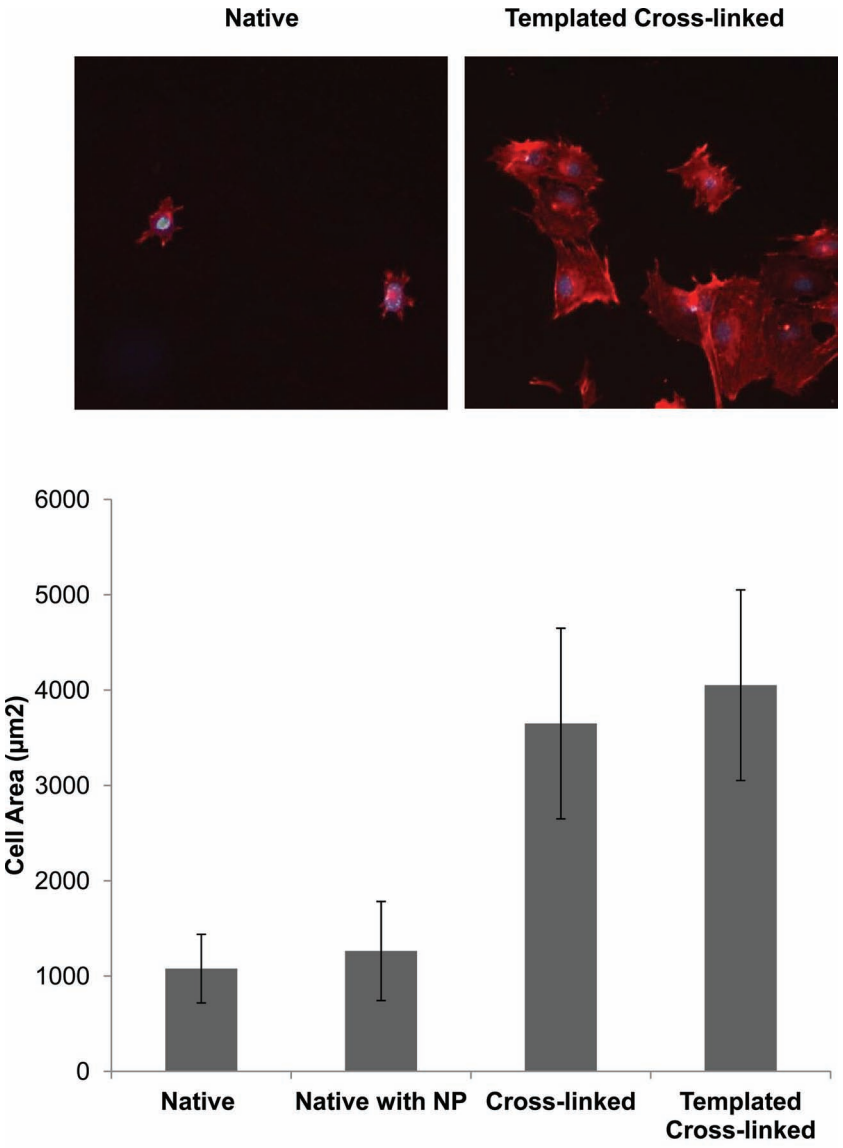

Figure 4. Representative cytoskeletal structures (top) and average cell area (bottom) of MC3T3-E1 cells cultured for 24 h on $(PLL\text{-}PGA)_{14}$ (native), $[(PLL\text{-}PGA)_5\text{-}PLL\text{-}NP]_2\text{-}(PLL\text{-}PGA)_2$ (native with NP), $(PLL\text{-}PGA)_{14}$ plus EDC/NHS(cross-linked), and $[(PLL\text{-}PGA)_5\text{-}PLL\text{-}NP]_2\text{-}(PLL\text{-}PGA)_2$ plus EDC/NHS plus THF (templated cross-linked) films. F-actin and nuclei are stained red and blue, respectively. Films formed at NP concentration 0.1 g/L.

dissolution step (right of Figure 6), exposure to red labeled albumin results in a yellow film with some red apparent at the outer film surface, and little red in the space above the film. This image suggests most of the solution albumin to enter the film. Rinsing then acts to remove all of the red color, but leaves the film partially yellow, indicating some of the albumin to remain in the film. These results suggest albumin to enter and distribute throughout most of the templated film (i.e., with template particles removed), but not the non-templated film (i.e., with template particles left in place), and thus provide strong evidence for the formation of accessible pore space via the templating strategy employed here. The presence of albumin throughout the film suggests the NP themselves to be fairly uniformly distributed prior to their removal. Based on a solution albumin concentration of 1 g/L, a 1 mm solution overlayer, and a film thickness of 10 μm, the loading and concentration within the templated film are 0.1 mg/cm^2 and 100 g/L, respectively, corresponding to about 10% of the overall film mass consisting of albumin. Note the good agreement with a NP volume fraction of 12%, estimated above from QCMD and ellipsometry data.

To quantify the extent and reversibility of biomolecular loading within NP templated LbL films, we show in **Figure 7** QCMD measurements of albumin adsorbed to/within templated and non-templated films, following a 30 minute adsorption step and a 10 minute buffer rinse. In all cases, the change in signal during the rinse is less than 5%, suggesting limited short-time reversibility. At lower albumin concentration (0.1 g/L), we observe little difference in resonator frequency shift between a non-templated film, and one templated at 0.1 g/L NP. However, a nearly two-fold signal increase is observed for a film templated at 1 g/L NP. At higher albumin concentration (1 g/L), both the 0.1 g/L and 1 g/L NP templated films exhibit signals roughly twice that of the non-templated film. These results suggest 1) albumin adsorption to occur at the surface of the non-templated films (as expected), and 2) significant additional adsorption to take place within the interior pore space of all templated films, except the one with low concentrations of both NP and albumin. Some care must be employed when estimating loading via QCMD frequency change; the signal is expected to be more sensitive to surface adsorption than to adsorption within the pore space, since in the latter case the increase in protein mass within the film is compensated somewhat by displacement of water. Nonetheless, these data clearly demonstrate successful creation of accessible pore space, and biomolecular loading that increases with extent of NP templating and biomolecular solution concentration.

3. Discussion

The present work is motivated by an important biomaterials challenge, namely, to independently optimize mechanical rigidity and bioactivity. Canonical methods employed to increase the former, e.g., covalent cross-linking of a gel matrix, tend to suppress the latter, and vice versa. Previously, we demonstrated a "surface cross-linking" strategy, resulting in LbL films with a rigid outer "skin" to enhance cell adhesion, that is

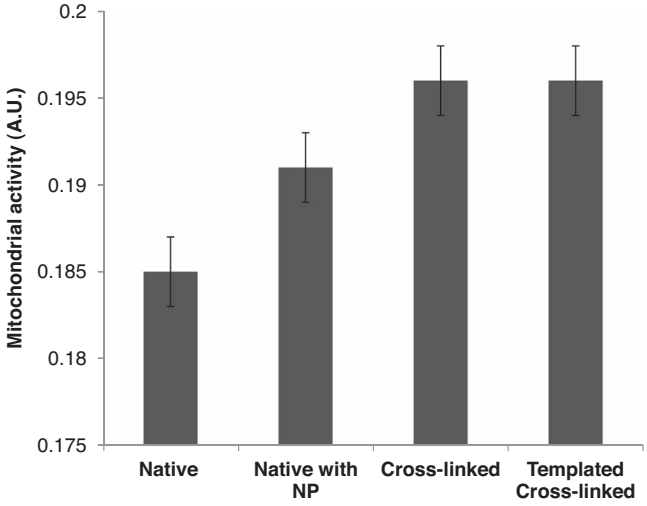

Figure 5. Alamar blue assay of 2 day MC3T3-E1 preosteoblast cell metabolic activity on $(PLL\text{-}PGA)_{14}$ (native), $[(PLL\text{-}PGA)_5\text{-}PLL\text{-}NP]_2\text{-}(PLL\text{-}PGA)_2$ (native with NP), $(PLL\text{-}PGA)_{14}$ plus EDC/NHS (cross-linked), and $[(PLL\text{-}PGA)_5\text{-}PLL\text{-}NP]_2\text{-}(PLL\text{-}PGA)_2$ plus EDC/NHS plus THF (templated cross-linked) films. Films formed at NP concentration 0.1 g/L.

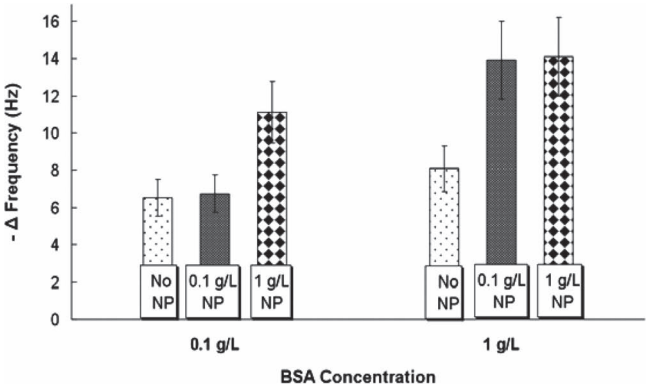

Figure 7. Quartz crystal microgravimetry measurements of bovine serum albumin (BSA) adsorption onto/within cross-linked, THF exposed $(PLL\text{-}PGA)_8$ (no NP) and $[(PLL\text{-}PGA)_2\text{-}PLL\text{-}NP]_2\text{-}(PLL\text{-}PGA)_2$ (0.1 and 1 g/L NP concentration) films.

sufficiently thin so as to minimally affect embedded biomolecules.[23] Here, we employ a nanoparticle templating strategy to create porous films, whose matrix may be made rigid through standard cross-linking techniques, and whose pore space may house bioactive species loaded after film assembly and cross-linking treatment. A particular advantage to this method is the possibility to stably embed biological species without regard to size. Previous reports show the successful loading of smaller drug[28] or protein[22,29,30] species into LbL films following standard chemical cross-linking treatments; our results suggest a molecule the size of albumin (of dimension 8 to 11 nm)[51] may only enter a cross-linked film possessing templated pore space (Figure 6).

Porous films capable of high biomolecular loading are promising materials for cell contacting applications. The idea is to achieve a high local concentration of bioactive agent near to the cell-material interface, such that cellular influence occurs via a direct contact (as opposed to a solution release) mechanism. Hammond et al. and Lynn et al. have demonstrated hydrolytically degradable LbL films acting via a solution release mechanism.[31,34,52–55] Picart and co-workers make the case that bioactive species such as growth factors, despite being typically administered via solution in vitro, are in fact generally immobilized in vivo,[32] and have shown bone morphogenetic protein embedded within an LbL film to sensitively control osteoblastic cell behavior.[29,30,32] By enabling the independent control of mechanical rigidity and bioactive species loading, our templating approach represents a potentially significant step toward films capable of controlling cellular fate.

Tissue engineering, a medical and engineering approach toward the replacement of lost or diseased tissue, represents an important potential application for the porous nanofilm biomaterials introduced here. A typical tissue engineering strategy involves seeding stem or progenitor cells within a porous scaffold device, allowing them to grow/mature in vitro, and then implanting them in vivo. Many common polymers used to form scaffold devices are weakly cytophilic, and may require surface modification, e.g., through LbL assembly of charged macromolecules.[34,56,57] Porous nanofilm biomaterials, as introduced here, offer the possibility of scaffold coatings capable of promoting strong initial cell adhesion, and

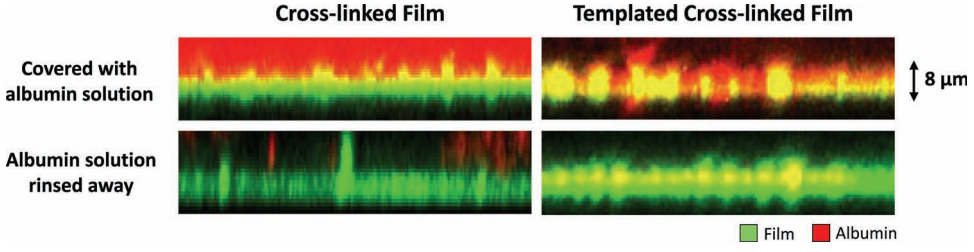

Figure 6. Laser scanning confocal microscopy images of cross-linked $[(PLL\text{-}PGA)_5\text{-}PLL\text{-}NP]_4\text{-}(PLL\text{-}PGA)_2$ films, without (left) and with (right) NP removed via THF exposure (films formed at NP concentration 1 g/L). PLL placed in the penultimate layer contains a FITC (green) label, and is expected to freely diffuse throughout the film.[50] When exposed to an Alexa Fluor (red) labeled albumin solution, the cross-linked film (left) appears green and the contacting solution red, suggesting impermeability of the film to albumin. Following a buffer rinse, most of the red disappears. When exposed to the albumin solution, the templated cross-linked film (right) appears yellow, suggesting penetration of albumin into the film. Following a buffer rinse, the film appears green and yellow, suggesting much of the albumin to remain in the film.

able to communicate biological signals to cells following their initial adhesion, both key attributes to promoting the formation of viable, functional tissue. Note the hierarchy of porosity considered here: macropores within the scaffold device house cells, and nanopores within the film coating the surface of the macropores house bioactive agents. As a specific example, consider bone tissue engineering, where previous success has been achieved with fibrous porous scaffolds formed via electrospinning or thermally induced phase separation of degradable polymers such as poly(lactic acid) and poly(glycolic acid).[46,58–60] As a scaffold pore space surface coating, a porous nanofilm biomaterial may be loaded with the growth factor bone morphogenetic protein (BMP), known to promote the proliferation and differentiation of osteoblastic precursor cells.[61] The choice here of MCT3T-E1 cells is motivated in part by this potential bone tissue engineering application. Previous studies have shown BMP immobilized by simple physical adsorption to a polymeric scaffold device to significantly enhance the osteogenic differentiation of seeded MCT3T-E1 cells.[60] Nanofilm biomaterials loaded with BMP offer the possibility to present BMP directly to contacting cells.[29,30,32] Porous nanofilm biomaterials, as presented here, allow for the independent control over film mechanical rigidity and bioactive species loading, and hence potentially for a higher level of control over the formation of bone tissue.

Although we consider only pre-osteoblastic cells here, the possibility also exists to employ porous nanofilm biomaterials with stem cells. Various soluble factors are known to influence the differential fate of stem cells, and could be embedded within porous films. Substrate rigidity is also known to direct stem cell fate: the group of Discher has demonstrated how myogenic, neurogenic, and osteogenic differentiation of mesenchymal stem cells may be favored simply by altering the stiffness of the underlying matrix.[62] By independently controlling mechanical rigidity and bioactivity, porous nanofilm biomaterials could prove especially useful toward directing stem cell differentiation.

Nanoparticle templating is an attractive means toward LbL films of controlled porosity, but other approaches exist as well. Mendelsohn et al. have shown an abrupt decrease in solution pH following LbL assembly to result in film expansion and the formation of an interconnected porous network, of characteristic pore size 100–500 nm, and a subsequent increase in solution pH to result in film contraction and the formation of discrete, vertical, film-spanning pores of 50–200 nm diameter.[63] The process is very sensitive to the pH of the precursor solutions, and a mechanism is proposed whereby suppressed polyanion ionization results in a loss of ionic cross-links, and ultimately to a spinodal decomposition-like pore-forming event. Such films have been investigated in solid electrolyte[64] and drug delivery[65] applications. Lutkenhaus et al. have shown how post-formation changes in solution conditions may lead to a rich array of LbL film pore structures, including the possibility of a gradient along the vertical direction, with pore sizes ranging from tens of nanometers to microns, and porosities from 0 to 77%.[66] Ultimately, both templating and "solution shock" pore forming strategies are likely to impact LbL film biomaterial applications.

4. Conclusion

We demonstrate here nanoparticle templating as a strategy toward thin film biomaterials of sufficient mechanical rigidity to promote strong initial cell adhesion, and capable of high bioactive species loading. Chemically cross-linked, nanoparticle templated, layer-by-layer assembled polyelectrolyte films promote an initial cellular response that is comparable to that of a non-templated film. In addition, they may be loaded with biomolecular species to a level of approximately 10% of the overall film mass. Independent control over mechanical rigidity and bioactivity may enable and enhance numerous cell contacting biomaterial applications.

5. Experimental Section

Quartz Crystal Microgravimetry with Dissipation (QCMD): A quartz crystal microbalance consists of a thin quartz disk sandwiched between a pair of electrodes. The resonant frequency of the crystal, when excited by an AC voltage, depends on the total oscillating mass, including coupled water. In addition, the dissipation may be measured at the fundamental and overtone frequencies. By applying a Voigt model of a viscoelastic medium–specifically, solving the wave equation for the shear displacement of the quartz element, a visco-elastic overlayer, and a purely viscous cover medium, with no-slip boundary conditions at the interfaces,[67] physical properties of the adhering film may be determined. A QCMD instrument (D300, Q-Sense, Sweden) was employed with a parallel plate flow cell whose bottom surface was a QSX 303 Sensor Chip (Q-Sense) consisting of a planar SiO_2 coating on a quartz crystal.

Ellipsometry: The ellipticity, or ratio of reflectivity of p- and s-waves of a polarized laser beam impinging on an interface, at angles near to the Brewster angle (i.e., where the p-wave reflectivity vanishes), yielded the thickness and refractive index of a macromolecular film. A PhE-101 Discrete Wavelength Ellipsometer (Angstrom Advanced Technologies) was employed on polyelectrolyte films formed on Si wafers.

Microscopy: Polyelectrolyte films (dried) were imaged via atomic force microscopy (Veeco Dimension 5000) in tapping mode. Cells adherent to films were imaged via optical microscopy (Leica) and digital photography (Canon Powershot S50). Permeation of fluorescently labeled species within films was imaged via laser scanning confocal microscopy (Biorad Model 1024).

Film Assembly, Cross-Linking, and THF Treatment: A QCMD sensor chip, silicon wafer, or glass microscope slide was washed with a 2% Hellmanex solution and rinsed with deionized water. In a QCMD experiment, the sensor chip was inserted into a flow cell and a PBS buffer solution was introduced under continuous flow (shear rate ca. s^{-1}) until a stable baseline appeared. 0.1 g L^{-1} PLL (MW 70–150 kDa, Sigma) and PGA (MW 50–100 kDa, Sigma) solutions were introduced alternately under continuous flow for 15 min exposure steps, separated by 5 min buffer rinse steps. In certain experiments, a solution of carboxyl functionalized latex nanoparticles (C37261, Invitrogen), of diameter 28 ± 4 nm, replaced some of the PGA solution exposures. In ellipsometry or microscopy experiments, a silicon wafer or glass slide was alternately dipped into 0.1 g L^{-1} PLL and PGA (or NP) solutions for 10 min exposure steps, separated by three 1 min buffer rinse steps. Chemical cross-linking was achieved via exposure to a 40 mM 1-ethyl-3-(3 (dimethylamino)propyl)-carbodiimide (EDC)-100 mM, *N*-hydroxysulfosuccinimide (sulfo-NHS) solution in buffer for 16 h, followed by a buffer rinse. Template particles were dissolved through exposure to tetrahydrofuran (THF) for 24 h, followed by three 20 min buffer rinses. In QCMD experiments, the sensor chip was then re-inserted into the flow cell, a buffer solution was introduced under continuous flow until a steady baseline was achieved, and a bovine serum albumin solution was introduced for 5 min, followed by a buffer rinse.

Fluorescence Labeling/Laser Scanning Confocal Microscopy (LSCM): A stock solution of Alexa Fluor 568 (AF 568) carboxylic acid succinimidyl ester (MW 792, Invitrogen) was prepared in anhydrous DMSO at 3.8 g L^{-1}. 10 µL of the AF solution was added to 1 mL of a 2 g L^{-1} bovine serum albumin (Sigma) solution in carbonate-bicarbonate basic buffer of pH 9.0. The mixture was incubated for 1 h at room temperature in the dark. The unbound dye was separated from the conjugate by gel filtration (Sephadex G-25, G2580 column, Sigma) and elution was performed with PBS at pH 7.4. Following film formation, crosslinking, and THF exposure on glass slides, films were exposed to 0.1 mL of the labeled albumin solution for 5 min. In certain cases, a buffer rinse followed.

Osteoblastic Attachment and Metabolic Activity Assays: Murine pre-osteoblastic MC3T3-E1 cells, established as an undifferentiated osteoblastic cell line from normal mouse calvaria, were grown in alpha minimal medium (Invitrogen) supplemented with 10% (v/v) decomplemented fetal bovine serum (PAA), glutamax (2 mM, Eurobio), penicillin (100 unit mL^{-1}, Eurobio), streptomycin (0.1 g L^{-1}, Eurobio). Cells were cultured in 75 cm^2 plastic culture flasks and incubated in a humidified incubator (37 °C and 5% CO_2). After 3 or 4 days of culture, freshly confluent (or sub-confluent) MC3T3-E1 pre-osteoblast cells were harvested with trypsin-EDTA solution 1:1 (v/v) and re-suspended in complete cell culture medium at 5000 cells cm^{-2} in a 48 well plate. After 3 h of culture, MC3T3-E1 pre-osteoblasts were visualized using a light microscope and optical microscopy images were taken using a digital camera. Cells were counted (n = 2 per well), and each condition was averaged. At 24 hours of culture, cells were fixed with 3% (w/v) para-formaldehyde solution dissolved in PBS (Sigma) for 15 min, then permeabilized with 1% (v/v) Triton X-100 (Sigma) for 15 min. Non-specific binding sites were blocked by incubating the substrates in PBS containing 1% Alb for 1 h. Nuclei were directly revealed with 0.1 g L^{-1} 4′ 6-diamidino-2-phenylindole dihydrochloride (DAPI, Sigma) and the cytoskeleton visualized with 0.05 g L^{-1} phalloidin-TRITC (Sigma), both diluted in PBS containing 0.1% Alb. Samples were then washed in PBS, mounted in mowiol, and examined using a Leica fluorescence microscope. Immunostaining was performed three times independently. Three random spot images of 0.4 mm^2 area, containing 10–15 cells, were obtained at 20× magnification from two repeated cell culture experiments. Cell outlines were detected using ImageJ image analysis software, and cell area was calculated based on the number of pixels covered by the cell. At 2 days of culture, an Alamar Blue assay was used to assess cell activity.[68] Alamar blue is a reagent converted by metabolically active cells into a colorimetric indicator. This assay thus provides an important measure of cellular metabolic activity. In brief, the culture medium was aspirated at the desired time, and 200 µL of fresh and complete medium containing 10% v/v Alamar Blue (Invitrogen) was added to all wells. Reagent blanks were included as well. Plates were returned to the incubator for 3 h at 37 °C prior to measuring the absorbance at 570 nm and 600 nm using a spectrophotometric plate reader. Absorbance readings were converted to dye reduction% as per the provider's instructions. Extent of dye reduction increased with cellular metabolic activity.

Acknowledgements

P.V.T. and E.P. contributed equally to the supervision of this work. The authors graciously acknowledge assistance with film assembly from M. Calhoun, D. Eggerman, and M. McMillan, and funding from the National Science Foundation (CBET-0756323). Facilities use was supported in part by the Yale Institute for Nanoscience and Quantum Engineering, and NSF MRSEC DMR-1119826.

Received: April 15, 2012
Revised: July 18, 2012
Published online: August 10, 2012

[1] G. Decher, *Science* **1997**, *277*, 1232.
[2] P. T. Hammond, *Adv. Mater.* **2004**, *16*, 1271.
[3] P. T. Hammond, *AIChE J.* **2011**, *57*, 2928.
[4] Z. Y. Tang, Y. Wang, P. Podsiadlo, N. A. Kotov, *Adv. Mater.* **2006**, *18*, 3203.
[5] C. Picart, *Curr. Med. Chem.* **2008**, *15*, 685.
[6] T. Boudou, T. Crouzier, K. F. Ren, G. Blin, C. Picart, *Adv. Mater.* **2010**, *22*, 441.
[7] V. Gribova, R. Auzely-Velty, C. Picart, *Chem. Mater.* **2012**, *24*, 854.
[8] J. D. Mendelsohn, S. Y. Yang, J. Hiller, A. I. Hochbaum, M. F. Rubner, *Biomacromolecules* **2003**, *4*, 96.
[9] L. Richert, F. Boulmedais, P. Lavalle, J. Mutterer, E. Ferreux, G. Decher, P. Schaaf, J. C. Voegel, C. Picart, *Biomacromolecules* **2004**, *5*, 284.
[10] L. Richert, A. J. Engler, D. E. Discher, C. Picart, *Biomacromolecules* **2004**, *5*, 1908.
[11] C. Picart, R. Elkaim, L. Richert, T. Audoin, Y. Arntz, M. D. Cardoso, P. Schaaf, J. C. Voegel, B. Frisch, *Adv. Funct. Mater.* **2005**, *15*, 83.
[12] M. T. Thompson, M. C. Berg, I. S. Tobias, M. F. Rubner, K. J. Van Vliet, *Biomaterials* **2005**, *26*, 6836.
[13] A. Schneider, G. Francius, R. Obeid, P. Schwinte, J. Hemmerle, B. Frisch, P. Schaaf, J. C. Voegel, B. Senger, C. Picart, *Langmuir* **2006**, *22*, 1193.
[14] A. Schneider, L. Richert, G. Francius, J. C. Voegel, C. Picart, *Biomed. Mater.* **2007**, *2*, S45.
[15] A. Schneider, C. Vodouhe, L. Richert, G. Francius, E. Le Guen, P. Schaaf, J. C. Voegel, B. Frisch, C. Picart, *Biomacromolecules* **2007**, *8*, 139.
[16] C. R. Wittmer, J. A. Phelps, W. M. Saltzman, P. R. Van Tassel, *Biomaterials* **2007**, *28*, 851.
[17] C. R. Wittmer, J. A. Phelps, C. M. Lepus, W. M. Saltzman, M. J. Harding, P. R. Van Tassel, *Biomaterials* **2008**, *29*, 4082.
[18] K. F. Ren, T. Crouzier, C. Roy, C. Picart, *Adv. Funct. Mater.* **2008**, *18*, 1378.
[19] J. Blacklock, T. K. Sievers, H. Handa, Y. Z. You, D. Oupicky, G. Z. Mao, H. Mohwald, *J. Phys. Chem. B* **2010**, *114*, 5283.
[20] J. Blacklock, A. Vetter, A. Lankenau, D. Oupicky, H. Mohwald, *Biomaterials* **2010**, *31*, 7167.
[21] S. Mehrotra, S. C. Hunley, K. M. Pawelec, L. X. Zhang, I. Lee, S. Baek, C. Chan, *Langmuir* **2010**, *26*, 12794.
[22] T. Boudou, T. Crouzier, C. Nicolas, K. Ren, C. Picart, *Macromol. Biosci.* **2011**, *11*, 77.
[23] J. A. Phelps, S. Morisse, M. Hindie, M. C. Degat, E. Pauthe, P. R. Van Tassel, *Langmuir* **2011**, *27*, 1123.
[24] N. Jessel, F. Atalar, P. Lavalle, J. Mutterer, G. Decher, P. Schaaf, J. C. Voegel, J. Ogier, *Adv. Mater.* **2003**, *15*, 692.
[25] N. Benkirane-Jessel, P. Lavalle, F. Meyer, F. Audouin, B. Frisch, P. Schaaf, J. Ogier, G. Decher, J. C. Voegel, *Adv. Mater.* **2004**, *16*, 1507.
[26] N. Benkirane-Jessel, P. Lavalle, E. Hubsch, V. Holl, B. Senger, Y. Haikel, J. C. Voegel, J. Ogier, P. Schaaf, *Adv. Funct. Mater.* **2005**, *15*, 648.
[27] N. Jessel, M. Oulad-Abdeighani, F. Meyer, P. Lavalle, Y. Haikel, P. Schaaf, J. C. Voegel, *Proc. Natl. Acad. Sci. USA* **2006**, *103*, 8618.
[28] C. Vodouhe, E. Le Guen, J. M. Garza, G. Francius, C. Dejugnat, J. Ogier, P. Schaaf, J. C. Voegel, P. Lavalle, *Biomaterials* **2006**, *27*, 4149.
[29] T. Crouzier, K. Ren, C. Nicolas, C. Roy, C. Picart, *Small* **2009**, *5*, 598.
[30] T. Crouzier, A. Szarpak, T. Boudou, R. Auzely-Velty, C. Picart, *Small* **2010**, *6*, 651.
[31] M. L. Macdonald, N. M. Rodriguez, N. J. Shah, P. T. Hammond, *Biomacromolecules* **2010**, *11*, 2053.

[32] T. Crouzier, L. Fourel, T. Boudou, C. Albiges-Rizo, C. Picart, *Adv. Mater.* **2011**, *23*, H111.
[33] T. Crouzier, F. Sailhan, P. Becquart, R. Guillot, D. Logeart-Avramoglou, C. Picart, *Biomaterials* **2011**, *32*, 7543.
[34] M. L. Macdonald, R. E. Samuel, N. J. Shah, R. F. Padera, Y. M. Beben, P. T. Hammond, *Biomaterials* **2011**, *32*, 1446.
[35] S. Pavlukhina, S. Sukhishvili, *Adv. Drug Delivery Rev.* **2011**, *63*, 822.
[36] N. J. Shah, J. Hong, M. N. Hyder, P. T. Hammond, *Adv. Mater.* **2012**, *24*, 1445.
[37] O. Etienne, A. Schneider, C. Taddei, L. Richert, P. Schaaf, J. C. Voegel, C. Egles, C. Picart, *Biomacromolecules* **2005**, *6*, 726.
[38] C. Picart, A. Schneider, O. Etienne, J. Mutterer, P. Schaaf, C. Egles, N. Jessel, J. C. Voegel, *Adv. Funct. Mater.* **2005**, *15*, 1771.
[39] F. Caruso, R. A. Caruso, H. Mohwald, *Science* **1998**, *282*, 1111.
[40] I. Pastoriza-Santos, B. Scholer, F. Caruso, *Adv. Funct. Mater.* **2001**, *11*, 122.
[41] D. B. Shenoy, A. A. Antipov, G. B. Sukhorukov, H. Mohwald, *Biomacromolecules* **2003**, *4*, 265.
[42] Q. Li, J. F. Quinn, F. Caruso, *Adv. Mater.* **2005**, *17*, 2058.
[43] Q. Li, J. F. Quinn, Y. J. Wang, F. Caruso, *Chem. Mater.* **2006**, *18*, 5480.
[44] K. Anselme, *Biomaterials* **2000**, *21*, 667.
[45] M. Hindie, M. C. Degat, F. Gaudiere, O. Gallet, P. R. Van Tassel, E. Pauthe, *Acta Biomater.* **2011**, *7*, 387.
[46] J. M. Holzwarth, P. X. Ma, *Biomaterials* **2011**, *32*, 9622.
[47] K. Naito, J. M. Yang, Y. Kagawa, *Mater. Sci. Eng. A* **2011**, *530*, 357.
[48] A. Citeau, J. Guicheux, C. Vinatier, P. Layrolle, T. P. Nguyen, P. Pilet, G. Daculsi, *Biomaterials* **2005**, *26*, 157.
[49] D. Cetin, A. S. Kahraman, M. Gumusderelioglu, *J. Biomater. Sci.* **2011**, *22*, 1157.
[50] C. Picart, J. Mutterer, L. Richert, Y. Luo, G. D. Prestwich, P. Schaaf, J. C. Voegel, P. Lavalle, *Proc. Natl. Acad. Sci. USA* **2002**, *99*, 12531.
[51] M. A. Kiselev, Y. A. Gryzunov, G. E. Dobretsov, M. N. Komarova, *Biofizika* **2001**, *46*, 423.
[52] K. C. Wood, H. F. Chuang, R. D. Batten, D. M. Lynn, P. T. Hammond, *Proc. Natl. Acad. Sci. USA* **2006**, *103*, 10207.
[53] C. M. Jewell, D. M. Lynn, *Adv. Drug Delivery Rev.* **2008**, *60*, 979.
[54] X. H. Liu, J. T. Zhang, D. M. Lynn, *Adv. Mater.* **2008**, *20*, 4148.
[55] R. M. Flessner, Y. Yu, D. M. Lynn, *Chem. Commun.* **2011**, *47*, 550.
[56] X. J. Sun, W. Peng, Z. L. Yang, M. L. Ren, S. C. Zhang, W. G. Zhang, L. Y. Zhang, K. Xiao, Z. G. Wang, B. Zhang, J. Wang, *Tissue Eng. Part A* **2011**, *17*, 2369.
[57] L. M. He, Y. F. Shi, Q. Han, Q. H. Zuo, S. Ramakrishna, W. Xue, L. B. Zhou, *J. Mater. Chem.* **2012**, *22*, 13187.
[58] Z. L. Lu, H. Zreiqat, *Tissue Eng. Part A* **2010**, *16*, 3075.
[59] J. R. Popp, K. E. Laflin, B. J. Love, A. S. Goldstein, *J. Tissue Eng. Regener. Med.* **2011**, *5*, 780.
[60] J. E. Kim, E. J. Lee, H. E. Kim, Y. H. Koh, J. H. Jang, *J. Biomed. Mater. Res. Part A* **2012**, *100A*, 1488.
[61] A. C. Allori, A. M. Sailon, S. M. Warren, *Tissue Eng. Part B* **2008**, *14*, 259.
[62] A. J. Engler, S. Sen, H. L. Sweeney, D. E. Discher, *Cell* **2006**, *126*, 677.
[63] J. D. Mendelsohn, C. J. Barrett, V. V. Chan, A. J. Pal, A. M. Mayes, M. F. Rubner, *Langmuir* **2000**, *16*, 5017.
[64] G. M. Lowman, H. Tokuhisa, J. L. Lutkenhaus, P. T. Hammond, *Langmuir* **2004**, *20*, 9791.
[65] M. C. Berg, L. Zhai, R. E. Cohen, M. F. Rubner, *Biomacromolecules* **2006**, *7*, 357.
[66] J. L. Lutkenhaus, K. McEnnis, P. T. Hammond, *Macromolecules* **2008**, *41*, 6047.
[67] M. V. Voinova, M. Rodahl, M. Jonson, B. Kasemo, *Phys. Scripta* **1999**, *59*, 391.
[68] G. R. Nakayama, M. C. Caton, M. P. Nova, Z. Parandoosh, *J. Immunol. Methods* **1997**, *204*, 205.